Journal of Alloys and Compounds 502 (2010) 439–444

Contents lists available at ScienceDirect

Journal of Alloys and Compounds

journal homepage: www.elsevier.com/locate/jallcom

Synthesis of protoporphyrin coated superparamagnetic iron oxide nanoparticles *via* dopamine anchor

Nurufe Kemikli [a], Huseyin Kavas [b], Sinan Kazan [c], Abdulhadi Baykal [a], Ramazan Ozturk [a,*]

[a] Department of Chemistry, Faculty of Arts and Science, Fatih University, Istanbul 34500, Turkey
[b] Department of Physics, Faculty of Arts and Science, Fatih University, Istanbul 34500, Turkey
[c] Department of Physics, Faculty of Science, Gebze Institute of Technology, Cayirova-Gebze, Kocaeli 41400, Turkey

ARTICLE INFO

Article history:
Received 12 March 2010
Received in revised form 20 April 2010
Accepted 25 April 2010
Available online 5 May 2010

Keywords:
Protoporphyrin IX
Dopamine
Fe_3O_4 nanoparticle
Magnetism

ABSTRACT

Dopamine conjugated protoporphyrin, PPD, was prepared by the coupling reaction of protoporphyrin IX and dopamine in the presence of dicyclohexylcarbodiimide (DCC) and N-hydroxysuccinimide (NHS) in DMF. The crude product was washed with ethanol–cyclohexane (1:1) mixture to remove dicyclohexylurea (DCU). Previously prepared Fe_3O_4 nanoparticles were coated with PPD (sub-7 nm monosize) by sonication in the methanol. The porphyrin coated Fe_3O_4 nanoparticles, PPDNP were separated by permanent magnet. The microstructure and magnetic properties of magnetic nanoparticles were characterized by XRD, TEM, FT-IR, and VSM. It is found that the nanoparticles have high crystallinity with distinct lattices and the magnetic measurements reveal their well-defined superparamagnetic behavior at room temperature.

1. Introduction

Protoporphyrin (PpIX) is the most reactive molecule among the porphyrinic photosensitizers towards to conjugate formation which is commonly used in photodynamic therapy (PDT) [1]. An approach to PDT of cancer, in preclinical and clinical studies, is based on the endogenous accumulation of protoporphyrin IX used as a precursor photosensitizer. Among them, protoporphyrin IX (which is a natural precursor of heme) as photosensitizer, binds to Fhit protein (fragile histidine triad) and its mutants in the active site in vitro inhibits the enzymatic activity of Fhit [2]. Kammerer et al. [3] have characterized the rescue response of human PC-3 prostate cancer cells exposed in vitro to sublethal PDT after 5-aminolevulinic acid-induced protoporphyrin IX sensitization at the transcriptome level using Affymetrix HG U133 Plus 2.0 oligonucleotide microarrays. To construct a molecular porphyrinic conjugate with the SPION (superparamagnetic iron nanoparticles) for potential applications in hyperthermia (HT) and PDT, protoporphyrin IX and magnetite (paramagnetic Fe_3O_4) are indispensable building blocks [4,5]. The enhancement of the accumulation of porphyrin photosynthesizers against biological substrates can be achieved by the conjugate formation with biomolecules (e.g. amino acids, proteins) [6,7]. For this purpose, ene-diol containing compounds (e.g. dopamine, catechol) are commonly in nature, playing important key roles in many biological reactions and in medical treatment and also results in altered optical properties of nanoparticles [8]. It is known that catechol acts as a chelating agent, forming tight bonds with iron oxides by converting the under-coordinated cationic iron surface sites to a bulk-like lattice structure [9]. Also, dopamine has the ability to replace the original capping ligand, oleylamine, on the Fe_3O_4 NPs surface and act as a robust anchor on the surface of Fe_3O_4 NPs. Moreover, the exceptional thermal stability of the dopamine-based anchor on the iron oxide surfaces satisfies the requirement of HT (hyperthermia) [10]. Xu et al. [11] used dopamine (DA) as a stable anchor to present functional molecules on the surface of iron oxide nanostructures.

Transition metal oxides have been of scientific and technological interest for many decades due to their interesting optical, magnetic, electrical and catalytical properties. Among these, magnetite (Fe_3O_4) is a common magnetic iron oxide that has a cubic inverse spinel structure [12–15]. The use of surface functionalized aqueous suspension of magnetite nanoparticles in clinical medicine has also intensified [16–18].

Magnetic nanoparticles are also used extensively in the field of biomagnetics for a broad range of applications, such as drug delivery [11,19–20], cell labeling and sorting [21], magnetic resonance imaging, sensing [22,23] as well as therapeutic applications [24] such as an AC magnetic field-assisted cancer therapy, i.e. hyperthermia, PDT [25]. Qu et al. [26] synthesized Fe_3O_4–chitosan nanoparticles used for hyperthermia (in this study glutaraldehyde was used to crosslink the chitosan). Gu et al. [9] reported the synthesis and cellular uptake of the conjugate of porphyrin and

* Corresponding author. Tel.: +90 212 866 3300/2072; fax: +90 212 866 3402.
E-mail address: rozturk@fatih.edu.tr (R. Ozturk).

0925-8388/$ – see front matter © 2010 Elsevier B.V. All rights reserved.
doi:10.1016/j.jallcom.2010.04.192

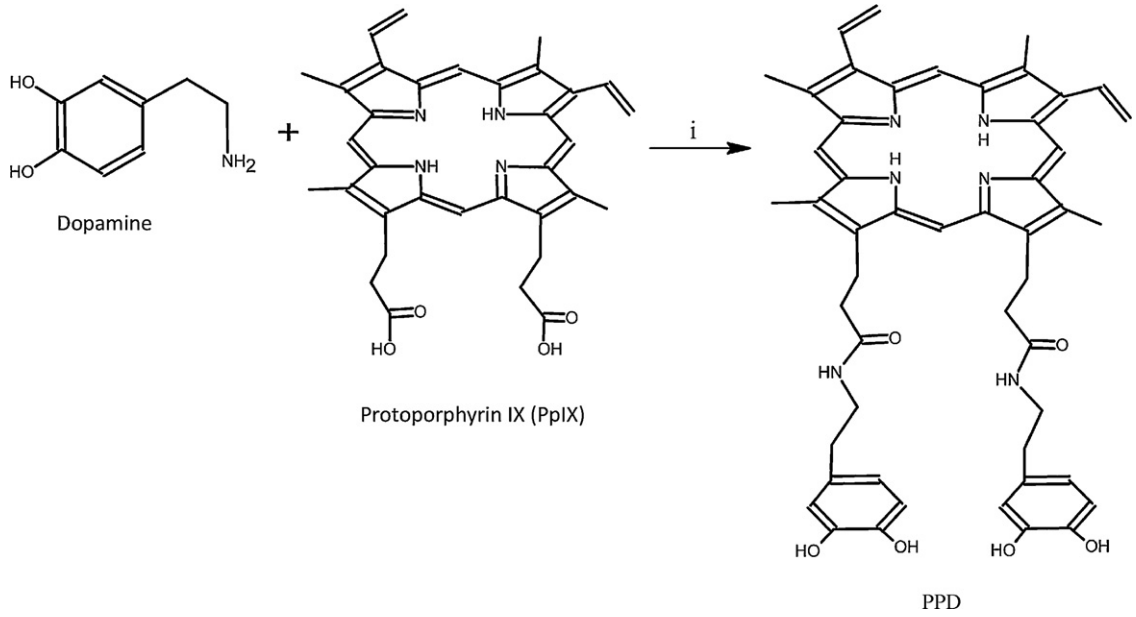

Scheme 1. Schematic representation of the synthesis of PPD; i: NHS, DCC, DMAP in DMF at RT, 3 h.

iron oxide nanoparticles, which may lead to a bimodal anticancer agent that can be used in the combinational treatment of photodynamic therapy (PDT) and hyperthermia therapy (HT). All these technological and medical applications require that the nanoparticles are superparamagnetic with sizes smaller than 15 nm with narrow-size distribution to have uniform physical and chemical properties [10].

In the present work, we describe the facile synthesis of dopamine conjugated protoporphyrin and its coating on Fe_3O_4 nanoparticles. All compounds have been characterized by TEM, XRD, NMR, FT-IR and magnetization studies.

2. Experimental

2.1. Materials

All commercial chemicals were used as supplied unless otherwise indicated. Chemicals, protoporphyrin IX was purchased from Frontierscientific, dopamine, dimethylaminopyridine (DMAP), dicyclohexylcarbodiimide (DCC), N-hydroxysuccinimide (NHS) were purchased from, Sigma and Alfa Aesar. The Fe_3O_4 nanoparticles having particle size <7 nm were synthesized according to given in the literature [5].

2.2. Instrumentation

X-ray powder diffraction (XRD) analysis was conducted on a Huber JSODebyeflex 1001 Diffractometer operated at 40 kV and 35 mA using Cu Kα radiation (λ = 1.54178 Å).

Fourier transform infrared (FT-IR) spectra were recorded in transmission mode with a PerkinElmer BX FT-IR infrared spectrometer. The powder samples were ground with KBr and compressed into a pellet. FT-IR spectra in the range 4000–400 cm^{-1} were recorded in order to investigate the nature of the chemical bonds formed.

^1H NMR spectra were recorded using a Bruker 400 MHz NMR spectrometer in DMSO (d_6-DMSO). Transmission electron microscopy (TEM) analysis was performed using a FEI Tecnai G2 Sphera microscope. A drop of diluted sample in alcohol was dripped on the TEM grid. Following drying, the sample was loaded into a TEM column for analysis. Particle size distribution was obtained from three micrographs, counting a minimum of 100 particles.

VSM measurements were performed by using a Quantum Design Vibrating sample magnetometer (QD-VSM). The sample was measured between ±5 kOe at room temperature and 10 K. ZFC (zero-field cooling) and FC (field cooling) measurements were carried out at 100 Oe and the blocking temperature was determined as 284 K. UV–vis absorption measurements were carried out with UNICAM-Helios in quartz cells.

2.3. Synthesis

2.3.1. Synthesis of dopamine conjugated protoporphyrin IX, PPD

The mixture of 100 mg of protoporphyrin IX (0.17 mmol), 100 mg DCC (0.484 mmol), 50 mg NHS (0.434 mmol) and catalytic amount of DMAP (2 mg, 0.016 mmol) in 10 ml of DMF was stirred under nitrogen at room temperature for about 3 h. 70 mg of dopamine (0.34 mmol) dissolved in 2 ml of DMF was added to this mixture and continued to stirring overnight. The mixture was filtered and the solvent was evaporated. The crude product was washed with ethanol–cyclohexane (1:1) mixture (20 ml) to remove dicyclohexylurea (DCU), which was formed during the coupling reaction, and excess dopamine and other reagents. The dark brownish colored product was obtained in a good yield (65%) (Scheme 1). ^1H NMR (d_6-DMSO, 400 MHz): δ 6.45 (d, 4H), 6.40 (d, 2H), 4.35 (s, 4H), 3.61 (t, 4H), 3.49 (t, 4H), 3.23 (t, 4H), 3.12 (t, 4H), 1.24 (s, 12H). ^{13}C NMR (d_6-DMSO, 400 MHz): δ porphyrin molecule (11.26, 25.23, 34.5, 119.00, 144.95, 172.81), dopamine (40.65, 115.3–115.8, 129.9, 143.38). MALDI-MS (*m*/*e*): calc.; 832.4, observed; 833.56.

2.3.2. Synthesis of porphyrin coated Fe_3O_4 nanoparticles, PPDNP

Monodisperse oleylamine-coated (particle size <7 nm) were synthesized by one-pot high temperature method and stored in hexane [5]. To modify the capping ligand on the Fe_3O_4 nanoparticles, 50 mg of protoporphyrin–dopamine conjugate was dissolved in 20 ml of chloroform–methanol (1:1) mixture was mixed with 300 mg oleylamine-coated Fe_3O_4 nanoparticles and sonicated for 45 min. Then 10 ml of hexane was added to the mixture and a permanent magnet was used to separate the magnetic nanoparticles. After repeating the washing steps two more times with hexane and followed by methanol the porphyrin coated nanoparticles were obtained (yield % 45) (Scheme 2).

3. Results and discussion

3.1. Characterization of dopamine conjugated protoporphyrin IX, PPD

In this study the dopamine conjugated protoporphyrin IX, PPD was obtained by the DCC coupling according to literature [9]. In the IR spectrum of PPD, the disappearance of C=O stretching peak of carboxylic acidic groups of protoporphyrin IX at 1695 cm^{-1} and appearance of the amide peaks of PPD at 1617 and 1519 cm^{-1} clearly indicate the conjugate formation. The amide N–H stretching bond (which is overlapping with the N–H stretching of porphyrin core) and the aromatic CH stretching peaks of the dopamine appeared at 3307 and 3090 cm^{-1}, respectively. In ^1H NMR spectra, many of the nuclei of protoporphyrin IX (PpIX) and dopamine were also observed in the spectrum of PPD. The vinylic and meso CH–protons of the PPD (which overlapped with the aromatic pro-

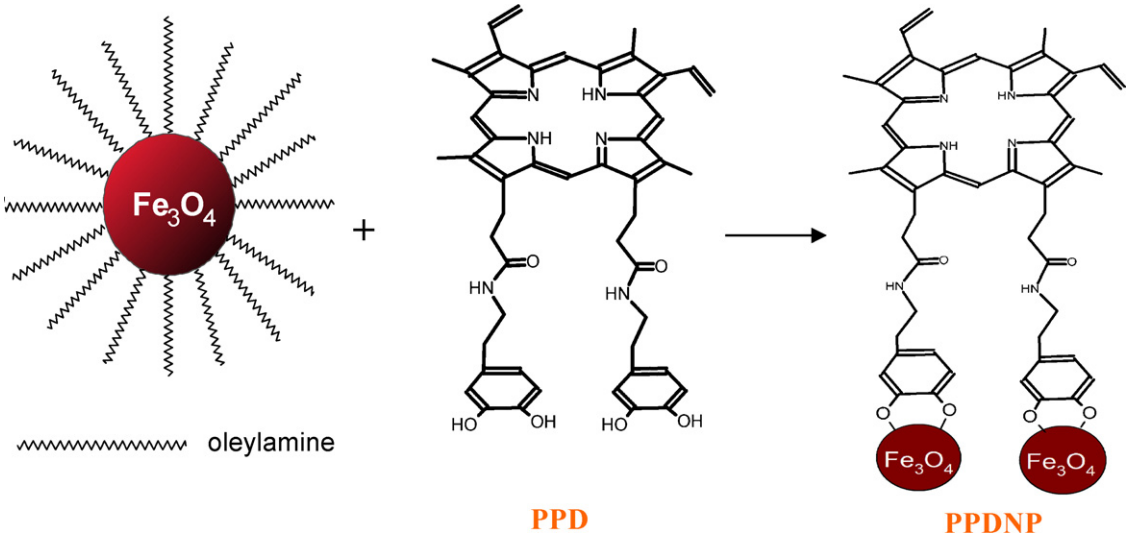

Scheme 2. Porphyrin coated Fe_3O_4 nanoparticles.

tons of dopamine groups) have approximately same shielding within the PpIX and appeared in the region of 6.40–6.45 ppm. The methyl groups of the porphyrin ring appeared at 24 ppm and CH_2 groups of ethyl chains in both porphyrin and dopamine appeared at 3.6 (t, 4H), 3.49 (t, 4H) and 3.23 (t, 4H), 3.2 (t, 4H) ppm, respectively. In ^{13}C NMR of the PPD, the peaks belonging to benzene group of the dopamine were realized in the ranges of 115.80–119.10 and 144.01–145.28 ppm. In the MALDI-MS spectrum of PPD, the molecular ion peak was seen at; 833.5 *m*/*e* (calc. 832.4 *m*/*e*). In the electronic absorption spectrum of PPD there is no any shifting in the absorption maxima since the dopamine conjugation does not affect the electronic absorption of the porphyrin core (Fig. 1). The B-band absorptions of protoporphyrin IX and PPD at around 404 nm indicate the identical porphyrinic cores.

3.2. Characterization of porphyrin coated Fe_3O_4 nanoparticles (SPION), PPDNP

3.2.1. XRD analysis

Phase investigation of the crystallized product was performed by XRD and the pattern is shown in Fig. 4. The XRD pattern indicates that the product is iron oxide, Fe_3O_4, and the diffraction peaks are broadened owing to small crystallite size. All the observed diffraction peaks could be indexed by the cubic structure of Fe_3O_4 (JCPDS no. 19-629) indicating a high phase purity of iron oxide. The broadening of the peaks in the present investigation is primarily attributed to the finite size of the ultra-small nanocrystals. On the basis of the Scherrer equation [27], using the width of most intense diffraction line, the average crystallite size for Fe_3O_4 was found as ~6 nm (Fig. 2).

3.2.2. FT-IR analysis

FT-IR spectra of oleylamine-coated SPION and porphyrin coated SPION (PPDNP) and PPD are shown in Fig. 3. Fig. 3a and b represents the characteristic peaks of SPION that are: metal–oxygen band, ν_1, observed at 590 cm^{-1} corresponds to intrinsic stretching vibrations of the metal at tetrahedral site ($Fe_{tetra} \leftrightarrow O$), whereas metal–oxygen band observed at 445 cm^{-1}, ν_2, is assigned to octahedral-metal stretching ($Fe_{octa} \leftrightarrow O$) [28–31]. Characteristic peaks for maghemite are not observed probably due to the overlap with wide absorption peaks of dominant magnetite phase. The spectral features of porphyrin are observed on porphyrin coated SPION by the presence of vibration bands at 1519, 1617, 1695, 3090 and 3307 cm^{-1}, respectively. These bands are absent in the spectrum of uncoated magnetite particles and confirm the presence of porphyrin on SPION.

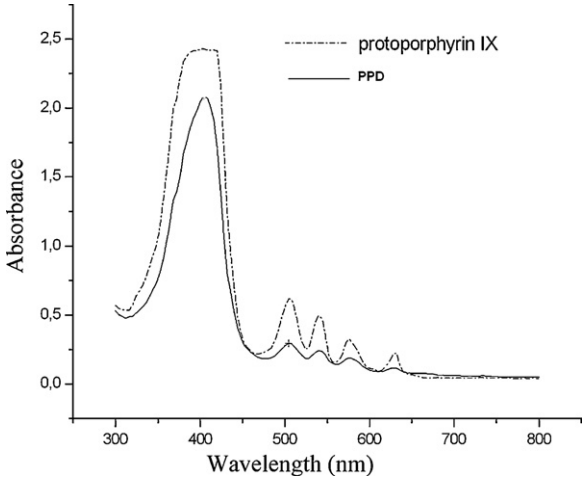

Fig. 1. Electronic absorption spectrum of PPD in DMSO.

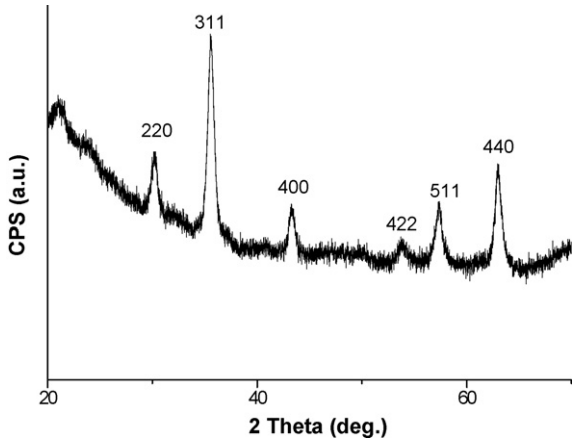

Fig. 2. X-ray powder diffraction pattern of porphyrin coated SPION.

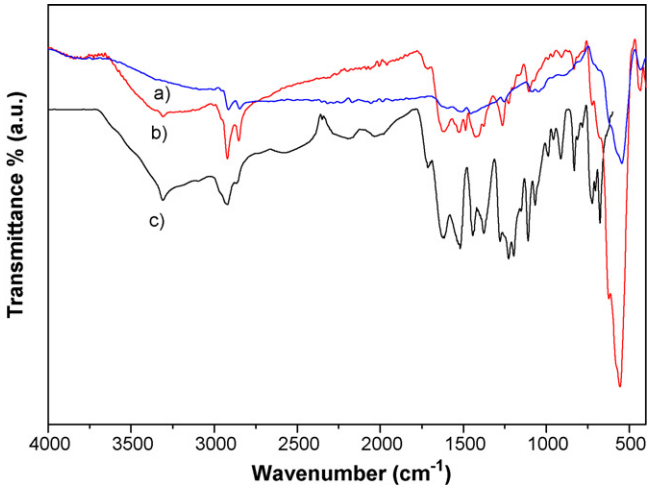

Fig. 3. FT-IR spectrum of (a) oleylamine-coated SPION, (b) porphyrin coated SPION (PPDNP), and (c) protoporphyrin–dopamine conjugate (PPD).

3.2.3. TEM analysis

The Fe_3O_4 nanoparticles coated with dopamine conjugated protoporphyrin IX were inspected by the TEM analysis (Fig. 4). In order to analyze the size distribution quantitatively, the particle size distribution was fitted using a log-normal function [32]. A mean diameter D_0, of 6.9 ± 0.2 nm was showing a good agreement with the crystallite size obtained from XRD peak broadening.

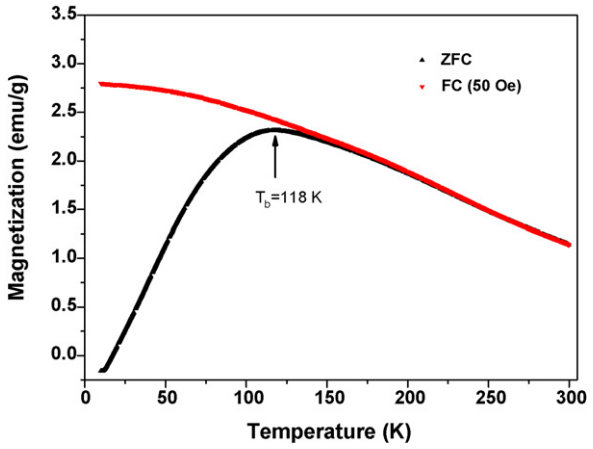

Fig. 5. Magnetization (M) versus temperature (T) measured in both FC and ZFC mode for porphyrin coated SPION.

3.2.4. VSM analysis

Fig. 5 shows the temperature dependence of magnetization in both field cooling (FC) and zero-field cooling (ZFC) mode for Fe_3O_4 composite nanoparticles. These two curves coincide initially and start separate from each other and follow different behaviors as the temperature decreasing from 300 to 10 K. The shape of FC and ZFC curves is the result of dipole–dipole interaction between the Fe_3O_4 nanoparticles. As shown in Fig. 5 the variation of the magnetization in FC and ZFC mode indicates the superparamagnetic behavior. The

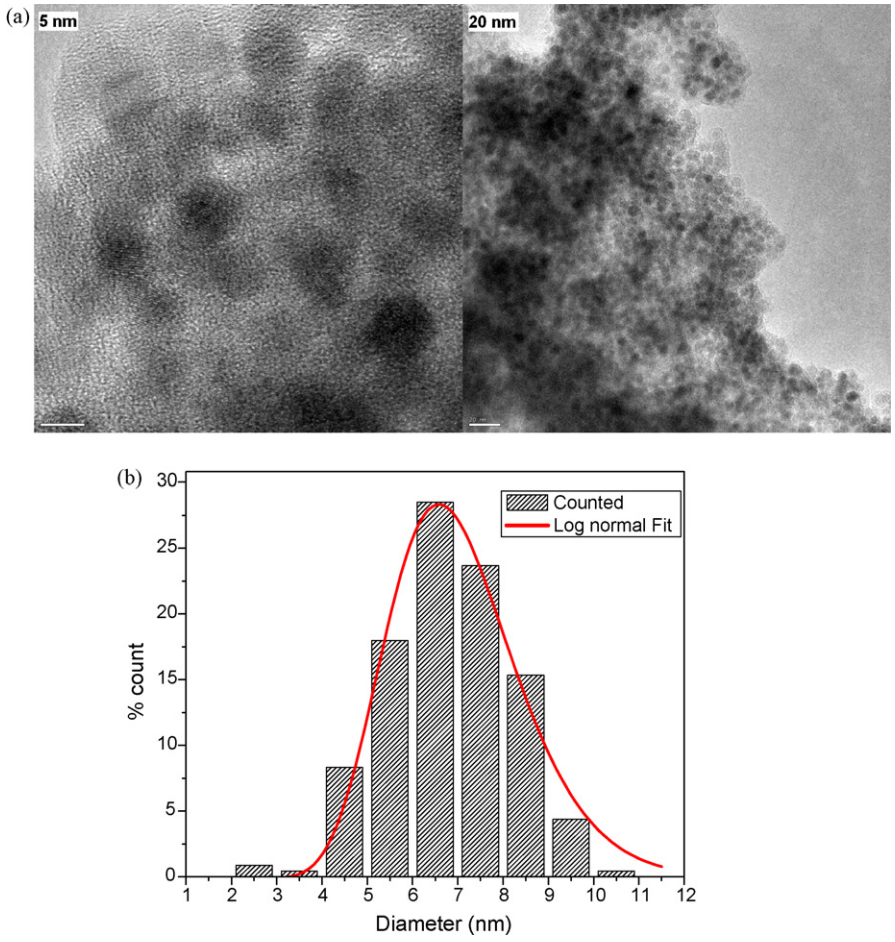

Fig. 4. TEM micrograph (a) porphyrin coated SPION and (b) calculated histogram.

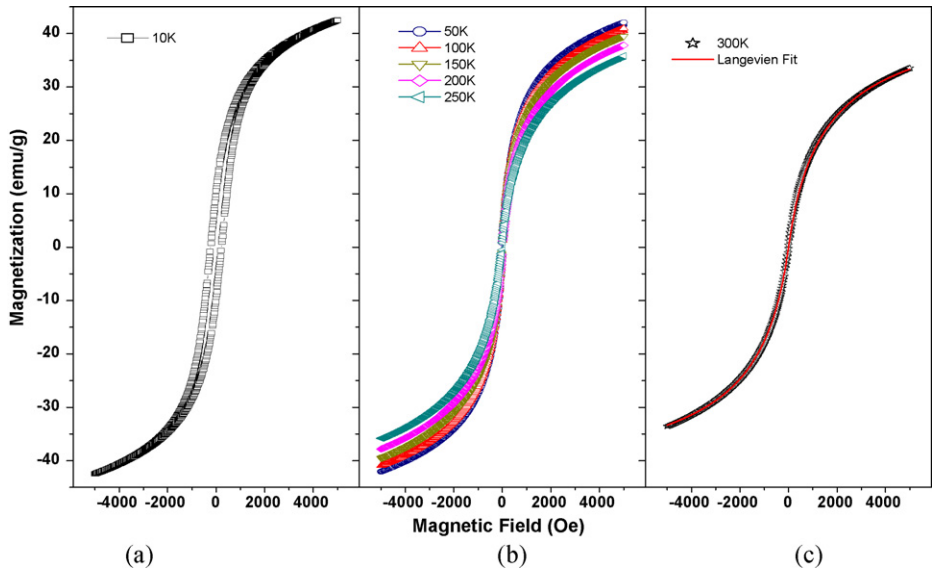

Fig. 6. Magnetization (M) as a function of magnetic field (H) at different temperature for porphyrin coated SPION.

maximum of the ZFC curves define the blocking temperature T_B (118 K), where the thermal energy becomes comparable with the anisotropy energy. For temperature below to T_B magnetization of each nanoparticle align in easy axis of their anisotropy. Due to the random orientation of easy axes of nanoparticles, the total magnetization approaches zero at low temperature. However when the sample warmed up to 300 K with small amount of field the particles gain thermal energy comparable to the anisotropy energy. So the magnetization switches to the direction of applied external field. This leads to increase in the magnetization of the sample. The value of blocking temperature was found as 118 K for Fe_3O_4 nanoparticles. The magnetic anisotropy constant was calculated by using $KV = 25k_BT$ (where k_B = Boltzman constant, V = volume of nanoparticle, and T_B = blocking temperature) and was found as 60.5×10^5 erg/cm^3. In the literature [33] Fe_3O_4 nanoparticles with a size of 8 and 11 nm have blocking temperature of 180 and 225 K, and corresponding magnetic anisotropy constants of 23.2×10^5 and 8.6×10^5 erg/cm^3, respectively. The different blocking temperature is attributed to the different size and the existence of a broadened distribution of energy barriers. In nanoparticles especially below 10 nm the magnetic anisotropy constant increases drastically while decreasing sizes. Large values of K in nanoparticles may be attributed to dipolar interactions for concentrated systems and surface effects mainly in diluted systems [34,35] (Fig. 5).

The M–H curve of nanoparticles shows nonhysteric characteristics at the temperature of 50, 100, 150, and 200 K (Fig. 6b) and at room temperature, 300 K (Fig. 6c) as expected for superparamagnetic systems. As it can be seen from Fig. 6a, when temperature has decreased to 10 K, a hysteric curve with a coercivity of 220 Oe and a lack of saturation were also observed at such a high magnetic field of 5 kOe. The extrapolated values of saturation magnetizations from M vs. $1/H$ curves while $1/H$ goes to zero decreases with increasing temperature and this behavior implies the co-existence of ferromagnetic interactions with saturation tendency and antiferromagnetic interactions with non-saturation tendency at high fields [36].

Nanoparticles with giant magnetic moment μ, can be represented by a Langevin function $L(x)$ of argument $x = \mu H/k_BT$. Based on the log-normal distribution of particle sizes obtained from TEM data, we use a distribution-weighted sum of Langevin functions [37]. From the fitting the particle size, standard deviation and saturation magnetization are found as 6.20 nm, 0.68 and 45.2 emu/g (234.5 emu/cm^3), respectively. The obtained particle size by Langevin fit, 6.2 nm is in close agreement with the size obtained from TEM micrographs, 6.89 nm. Yielded saturation value M = 45.2 emu/g, much smaller than the expected 85–95 emu/g for bulk magnetite which may be attributed to the spin canting effect as discussed above.

4. Conclusion

We have obtained monosize sub-7 nm porphyrin coated magnetite nanoparticles. The results from the structural characterization and magnetic measurements show that the magnetic nanoparticles have high crystallinity with distinct lattices and well-defined superparamagnetic behavior at room temperature. These monodispersed porphyrin coated Fe_3O_4 nanoparticles with tailorable size and tunable magnetic properties are promising for biomedical applications such as MRI and biosensors. Biological application of synthesized product is now in progress and results will be published as separate study.

Acknowledgements

The authors are thankful to the Fatih University Research Project Foundation (P50020602 and P50020902-2) and the Ministry of Industry of Turkey (San Tez project no. 00185.STZ.2007-2) for financial support of this study.

Appendix A. Supplementary data

Supplementary data associated with this article can be found, in the online version, at doi:10.1016/j.jallcom.2010.04.192.

References

[1] D.K. Chatterjee, L.S. Fong, Y. Zhang, Adv. Drug Deliv. Rev. 60 (2008) 1627.
[2] J. Pankau, A. Kowalska, N. Issaeva, A. Burcza, P. Kwiek, N. Bednarz, A. Pramanik, B. Banecki, A.J. Podhajska, J. Photochem. Photobiol. B 86 (1) (2007) 35.
[3] R. Kammerer, P. Pallucha, K. Oboukhovskij, M. Toelge, T. Pongratz, W. Beyer, A. Buchner, R. Baumgartner, W. Zimmermann, Med. Laser Appl. 24 (2009) 237.
[4] K.P. Liem, R.J. Mart, S.J. Webb, J. Am. Chem. Soc. 129 (2007) 12080.
[5] K.L. Young, Y.C. Xu, J. Xie, S. Sun, J. Mater. Chem. 19 (2009) 6400.
[6] V. Sol, P. Branland, V. Chaleix, R. Granet, M. Guilloton, F. Lamarche, B. Verneuil, P. Krausz, Bioorg. Med. Chem. Lett. 14 (2004) 4207.

[7] M. Kwitniewski, D. Kunikowska, B.D. Pietrzak, H. Dziadziuszko, A. Graczyk, R. Glosnicka, J. Photochem. Photobiol. B 81 (2005) 129.
[8] T. Rajh, L.X. Chen, K. Lukas, T. Liu, M.C. Thurnauer, D.M. Tiede, J. Phys. Chem. B 106 (2002) 10543.
[9] H. Gu, K. Xu, Z. Yang, C.K. Chang, B. Xu, Chem. Commun. 34 (2005) 4270.
[10] A.K. Gupta, M. Gupta, Biomaterials 26 (18) (2005) 3995.
[11] C. Xu, K. Xu, H. Gu, R. Zheng, H. Liu, X. Zhang, Z. Guo, B. Xu, J. Am. Chem. Soc. 126 (2004) 9938.
[12] R.M. Cornell, U. Schwertmann, The Iron Oxides: Structure, Properties, Reactions Occurrence and Uses, VCH, New York, 1996, pp. 28–29.
[13] T. Ozkaya, Synthesis and characterization of M_3O_4 (M: Fe, Mn, Co) magnetic nanoparticles, Master Thesis, Fatih University, Istanbul-Turkey, 2008.
[14] Z. Durmus, H. Kavas, M.S. Toprak, A. Baykal, T.G. Altıncekic, A. Aslan, A. Bozkurt, S. Cosgun, J. Alloys Compd. 484 (2009) 371.
[15] Z. Durmus, Synthesis and characterization of coated magnetic spinel nanoparticles, Master Thesis, Fatih University, Istanbul-Turkey, 2009.
[16] Z. Li, Z. Chen, H. Bao, M. Gao, Chem. Mater. 16 (2004) 1391.
[17] S. Si, A. Kotal, T.K. Mandal, S. Giri, H. Nakamura, T. Kohara, Chem. Mater. 16 (2004) 3489.
[18] D. Caruntu, G. Caruntu, Y. Chen, C.Y. O'Connor, G. Goloverda, V.L. Kolesnichenko, Chem. Mater. 16 (2004) 5527.
[19] O. Veiseh, J.W. Gunn, M. Zhang, Adv. Drug Deliv. Rev. 62 (2010) 284.
[20] C. Sun, J.S.H. Lee, M. Zhang, Adv. Drug Deliv. Rev. 60 (2008) 1252.
[21] H. Ito, R. Kato, K. Ino, H. Honda, J. Biosci. Bioeng. 109 (2) (2010) 182.
[22] T.K. Jain, S.P. Foy, B. Erokwu, S. Dimitrijevic, C.A. Flask, V. Labhasetwar, Biomaterials 30 (2009) 6748.
[23] F. Yang, Y. Li, Z. Chen, Y. Zhang, J. Wu, N. Gu, Biomaterials 30 (2009) 3882.
[24] B.B. Yellen, Z.G. Forbes, D.S. Halverson, G. Fridman, K.A. Barbee, M. Chorny, R. Levy, G. Friedman, J. Magn. Magn. Mater. 293 (2005) 647.
[25] D.L. Zhao, X.X. Wang, X.W. Zeng, Q.S. Xia, J.T. Tang, J. Alloys Compd. 477 (2009) 739.
[26] J. Qu, G. Liu, Y. Wang, R. Hong, Adv. Powder Technol. (2010), doi:10.1016/j.apt.2010.01.008.
[27] N. Kasapoglu, B. Birsöz, A. Baykal, Y. Koseoglu, M.S. Toprak, Cent. Eur. J. Chem. 5 (2007) 570.
[28] S. Wei, Y. Zhu, Y. Zhang, J. Xu, React. Funct. Polym. 66 (2007) 1272.
[29] R.A. Nyquist, R.O. Kagel, Infrared Spectra of Inorganic Compound, Academic Press, New York, 1971.
[30] I.J. Bruce, J. Taylor, M. Todd, M.J. Davies, E. Borioni, C. Sangregorio, T. Sen, J. Magn. Magn. Mater. 284 (2004) 145.
[31] T. Ozkaya, M.S. Toprak, A. Baykal, H. Kavas, Y. Köseoğlu, B. Aktaş, J. Alloys Compd. 472 (2009) 18.
[32] T. Kim, M. Shima, J. Appl. Phys. 101 (2007), 09M516.
[33] Y. Hou, J. Yu, S. Gao, J. Mater. Chem. 13 (2003) 1983.
[34] G.F. Goya, IEEE Trans. Magn. 38 (2002) 2610.
[35] F. Luis, F. Petroff, J.M. Torres, L.M. García, J. Bartolomé, J. Carrey, A. Vaurès, Phys. Rev. Lett. 88 (2002) 217205.
[36] D. Fiorani, S. Vitiocoli, J.L. Dorman, J.L. Tholence, A.P. Murani, Phys. Rev. B 30 (1984) 2776.
[37] H. Kavas, A. Baykal, M.S. Toprak, Y. Köseoglu, M. Sertkol, B. Aktas, J. Alloys Compd. 479 (2009) 49.